Earth, Planets and Space

FULL PAPER Open Access

Analysis of ionospheric storm-time effects over the East African sector during the 17 March 2013 and 2015 geomagnetic storms

Valence Habyarimana[1*], John Bosco Habarulema[2] and Teshome Dugassa[3]

Abstract

An analysis of the mechanisms that caused the storm-time effects during two geomagnetic storms that occurred on 17 March 2013 and 2015 is presented. We used Global Navigation Satellite System (GNSS) derived Total Electron Content (TEC) data over the trough (Addis Ababa, ADIS, 38.8°E geographic longitude, 0.18°N geomagnetic latitude) and near the crest (Mbarara, MBAR, 30.7°E geographic longitude, 10.22°S geomagnetic latitude) regions of East African sector. Magnetometer data over Addis Ababa (AAE) and Mbour (MBO) were also used to derive the disturbance in ionospheric currents during the two storm periods. The monthly median TEC values for a month within which the storm under consideration occurred were used as a measure of background variability to analyse the response of the ionosphere to the storms. The response of the ionosphere to a geomagnetic storm is considered to be significant when the magnitude of TEC deviation ($|\Delta TEC|$) is $\geq 45\%$. During the storm main phase, the ionosphere over the East African trough responded positively to the 17 March 2015 geomagnetic storm at 1800 UT, whilst at the crest regions, there was no significant response to the two St. Patrick's day geomagnetic storms. However, during the storm recovery phase of 17 March 2013 and 2015 storms, both the stations over the trough and crest regions of East Africa showed a positive response. We checked thermospheric $[O]/[N_2]$ changes as a result of the two storms. There were no appreciable changes in $[O]/[N_2]$ over this sector between 16 and 18 March 2013. We observed an appreciable change in $[O]/[N_2]$ between 16 and 18 March 2015. The $[O]/[N_2]$ increase was more pronounced/obvious on 18 March 2015. The positive ionospheric responses during the recovery phases of the two geomagnetic storms could not be attributed to changes in thermospheric $[O]/[N_2]$ because the responses were nighttime features. The southward turning of the z component of Interplanetary magnetic field (IMF *Bz*) led to enhanced eastward equatorial electric field (EEF) during 0725 UT (1025 LT) and 0645 UT (0945 LT) for 17 March 2013 and 17 March 2015 storms, respectively. We note that when the IMF *Bz* turned northward, the EEF turned westward. During the southward turnings of IMF *Bz* that took place at about 1435 UT (1735 LT) on 17 March 2013, eastward prompt penetration electric field (PPEF) occurred in the post-sunset period starting at about 1600 UT (1900 LT) and enhanced the Prereversal enhancement (PRE). The presence of westward PPEF at around 1500 UT (1800 LT) acted to suppress the PRE on 17 March 2015. The positive storm effects during the recovery phases of the two storms may be attributed to strong disturbed dynamo electric field (DDEF), which was eastward during the night. We may thus surmise that the ionospheric responses to geomagnetic storms of St. Patrick's day over the equatorial and low-latitude region of Africa were as a result of the combined effect of equatorward neutral wind, PPEF and DDEF.

Keywords Ionospheric storms, Total electron content, Ionospheric currents, Geomagnetic storms, Prompt penetration electric field, Disturbed dynamo electric field

*Correspondence:
Valence Habyarimana
valencehabyarimana@gmail.com
Full list of author information is available at the end of the article

Graphical Abstract

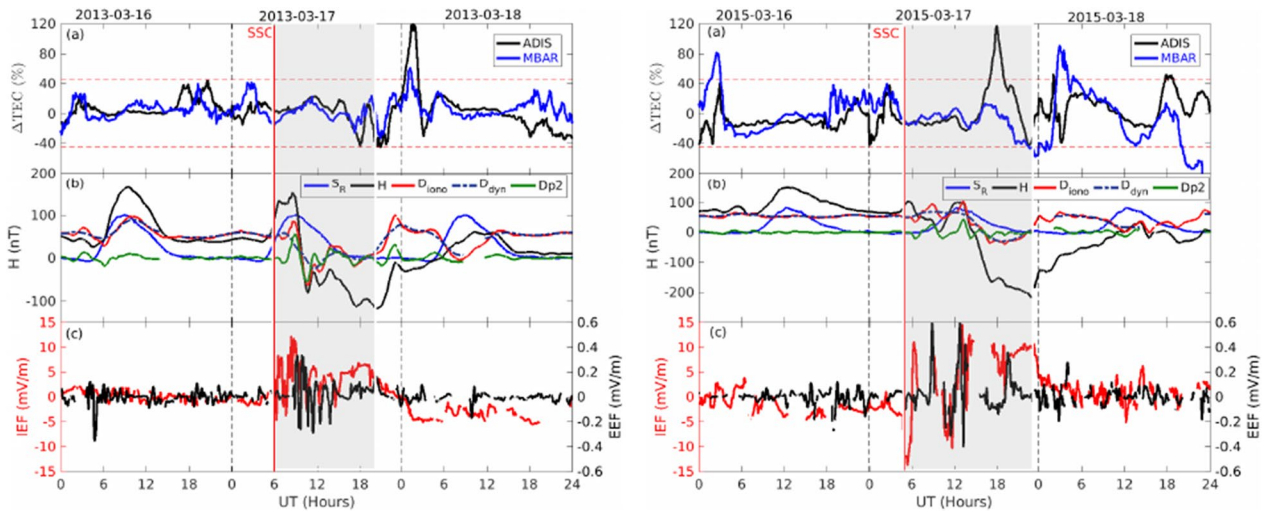

Introduction

The temporary disturbance in the Earth's magnetosphere is termed a geomagnetic storm. Geomagnetic storms are caused by streams of particles from the Sun that hit the Earth's magnetosphere driven by coronal mass ejections (CMEs) or corotating interaction regions (CIRs) (Gonzalez et al. 1994, 1999; Moldwin 2008). The CMEs can be visualised as bright features emanating from the solar corona at speeds between 10 km/s and 2000 km/s (Hundhausen 1999). The CMEs expel large quantities of plasma from the corona. The CIRs are long-lasting large-scale plasma structures generated in low and mid-latitude regions of the heliosphere through the interaction of a stable fast solar wind stream with the surrounding slow solar wind (Heber et al. 1999). During geomagnetic storms, the behaviour of ionosphere can be altered leading to either an increase or decrease in plasma density (Rishbeth 1963; McNamara 1991; Moldwin 2008). An increase/decrease in plasma density is termed as a positive/negative ionospheric storm (Rishbeth 1963; Danilov and Morozova 1985; Schunk and Sojka 1996; Balan et al. 2013; Horvath and Lovell 2015; Matamba et al. 2015). The ionosphere responds to a particular geomagnetic storm differently based on the time of sudden storm commencement (SSC), season, solar activity and the latitude region within which the ionosphere is found (Prölss 1995; Gao et al. 2008; Vijaya Lekshmi et al. 2011). During a geomagnetic storm, the ionosphere is highly variable and this degrades the high frequency (HF) radio communication. During a solar flare event, X-rays are directed towards the Earth and they knock off electrons from the atoms in the ionosphere creating an abnormally high density of free electrons in the lower ionosphere. The high density of free electrons (also known as sudden ionospheric disturbance) absorbs the HF radiowaves resulting into a blackout in HF communications and in transionospheric Global Navigation Satellite System (GNSS)-based timing and positioning for minutes to hours (e.g. Kintner et al. 2007; Basu et al. 2010; van der Meeren et al. 2014; Horvath and Lovell 2015). Therefore, understanding the influence of space weather phenomena on the ionosphere is of paramount importance. In addition, the response of the ionosphere to geomagnetic storms is relevant to system researchers and model developers as it helps them to characterise the generation or inhibition of ionospheric irregularities during space weather events (Sahai et al. 2009; Horvath and Lovell 2015).

Vertical $\mathbf{E} \times \mathbf{B}$ drift is one of the parameters that influence the variability of the ionosphere and thus responsible for storm-time effects and Rayleigh–Taylor instability, especially in equatorial/low latitudes (Sekar and Raghavarao 1987). When plasma is lifted upwards to altitudes where recombination rate is low, photoionisation takes place in the bottom ionosphere leading to the production of the new plasma that replaces the uplifted one (e.g. Kelley 1989). Vertical $\mathbf{E} \times \mathbf{B}$ drift is modified by prompt penetration electric field (PPEF) and neutral wind as a result of storm-related activity

(Balan et al. 2009, 2010). Depending on the configuration of PPEF, which is eastward during the day and westward at night, the orientation and magnitude of vertical $\mathbf{E} \times \mathbf{B}$ drift is modified resulting in significant increase or decrease in plasma density which could also affect the generation or inhibition of irregularities during post-sunset hours. During a strong daytime eastward PPEF event, the equatorial plasma fountain rapidly develops into a super-fountain due to the effect of equatorward neutral wind that affects plasma diffusion and raises the ionosphere to higher altitudes with reduced recombination rates (Kelley et al. 2004; Balan et al. 2009). Thus, the mechanical effects of the equatorward neutral wind combined with the PPEF event are responsible for positive ionospheric storms (e.g.Werner et al. 1999; Lin et al. 2005; Gonzalez et al. 2005; Lei et al. 2008; Balan et al. 2009, 2010; Matamba et al. 2015; Liu et al. 2016; Dugassa et al. 2019). The other possible cause of positive ionospheric storms include travelling atmospheric disturbances (TADs), which are manifested as travelling ionospheric disturbances (TIDs) (Ngwira et al. 2012; Amabayo et al. 2012; Habarulema et al. 2013). On the other hand, the disturbed dynamo electric field (DDEF) is westward/eastward during daytime/nighttime and results in a decrease/increase in plasma density within the ionosphere depending on the prevailing conditions (Tsurutani et al. 2004; Fuller-Rowell et al. 2002). In addition, during geomagnetic storms over the geomagnetic equator, strong PPEF alone can cause only negative effects in ionospheric density (e.g. Balan et al. 2009, 2010). Negative ionospheric effects during geomagnetic storms can as well be attributed to changes in neutral composition arising from Joule heating in the auroral oval which decreases the thermospheric $[O]/[N_2]$ ratio in the F2 region (e.g. Danilov and Morozova 1985; Liu et al. 2016), the equatorward migration of the mid-latitude electron density trough from high to low latitudes (e.g. Mendillo et al. 1974) and the enhanced fountain effect over the magnetic equator which results in a trough (region of decreased electron density) along the magnetic equator (e.g. Zhao et al. 2005; Liu et al. 2010).

The two St. Patrick's day geomagnetic storms have been studied extensively by Astafyeva et al. (2015); Hairston et al. (2016); Yue et al. (2016); Borries et al. (2016); Nava et al. (2016); Liu et al. (2016); Shreedevi and Choudhary (2017); Habarulema et al. (2018); Amaechi et al. (2018); Omojola and Adewumi (2020); and Feng et al. (2021) amongst others. For example, Astafyeva et al. (2015) used multi-instruments to study the 17–18 March 2015 ionospheric response over the American, African and Asian sectors. They observed hemispheric asymmetries in the ionospheric response. These asymmetries were attributed to changes in thermospheric composition and nondipolar positions of the geomagnetic field. Hairston et al. (2016) used five operational polar-orbiting Defense Meteorological Satellite Program (DMSP) satellites together with equatorial orbiting C/NOFS (Communication/Navigation Outage Forecasting System) satellite to infer the regional ionospheric responses to March 2015 St. Patrick's day storm. Yue et al. (2016) used ionospheric electron density reanalysis algorithm to generate global optimised electron density during 17–18 March 2013 geomagnetic storm. They assimilated both low earth orbit satellites-based and ground GNSS-TEC into a background ionospheric model. They were able to identify large-scale ionospheric features quite well during the phases of the geomagnetic storm. Borries et al. (2016) studied deviations in the European–African sector observed in TEC during March 2015 St. Patrick's day storm. Wavelike phenomena were observed which were signatures of large-scale TIDs. Similarly, Habarulema et al. (2018) used GNSS-TEC data over the American, African and Asian regions to study large scale TIDs during the storm of 16–18 March 2015. The authors attributed the poleward TIDs to Lorentz coupling from vertical $\mathbf{E}\times\mathbf{B}$ drift which gets enhanced during local daytime if there is an additional electric field, such as from PPEF as a result of southward turning of z component of interplanetary magnetic field (IMF *Bz*). Shreedevi and Choudhary (2017) observed a positive ionospheric storm effect over the Indian sector during the storm of 17 March 2013 near the equatorial/low-latitude region. Amaechi et al. (2018) carried out a simultaneous comparison of the two St. Patrick day geomagnetic storms of 2013 and 2015 in terms of scintillations, equatorial plasma bubbles (EPBs) and TEC irregularities. In their study, the response of the ionosphere to the geomagnetic storms was only considered during the main phase. In this study, a storm period (initial, main and recovery phases) was used to track the ionospheric effects and their driving mechanisms. Recently, Omojola and Adewumi (2020) studied the effects of St. Patrick's day geomagnetic storms of 2013 and 2015 using two GNSS stations over Nigeria. They observed variations in TEC which corresponded to variations in the positioning error arising from the latitudinal variation between the two stations considered in their study.

All these studies looked at the two storms in isolation, yet they occurred on the same day of the year and in the same season, though in different years. It is well known that the response of the ionosphere to different geomagnetic storms varies significantly from one storm to another since every storm condition can be highly localised (Kakad et al. 2012; Nayak et al. 2017). However, there may be some instances where two different storms may present common features (Kashcheyev et al. 2018).

In this study, we focus on the simultaneous observations and interpretation of the driving mechanisms that caused the response of the ionosphere over the East African equatorial and low-latitude region during St. Patrick's day geomagnetic storms of 17 March 2013 and 2015. The role played by ionospheric currents on the response of ionosphere to these selected geomagnetic storms is scrutinised. The impetus for this study is to carry out a simultaneous presentation of these storms and identification of their differences and/or similarities since they occurred during the same period and season.

Data and methods

In this study, ionospheric storm effects were analysed using GNSS-derived TEC data over Addis Ababa (ADIS, 38.8°E geographic longitude, 0.18°N geomagnetic latitude) and Mbarara (MBAR, 30.7°E geographic longitude, 10.22°S geomagnetic latitude). The Receiver INdependent EXchange (RINEX) data files over ADIS and MBAR (archived on https://data.unavco.org/archive/gnss/rinex/obs/) during the two selected storm periods were processed using Global positioning system (GPS)-TEC algorithm developed at Boston College (Seemala and Delay 2010; Seemala and Valladares 2011) to obtain GNSS-derived TEC. An elevation cutoff of 30° was adopted to minimise multipath effects on vertical TEC (VTEC). The VTEC data that was used in this study was averaged to 5 min cadence to remove small fluctuations that may be captured during the VTEC measurements.

Previously, ionospheric storms over the mid-latitude region were regarded as those whose magnitude of the percentage TEC deviation was greater or equal to 40% (e.g. Matamba et al. 2015). However, the ionosphere over the low-latitude region is more turbulent than that over the mid-latitude region (e.g. Molchanov 2004; Hobara et al. 2005; Amabayo et al. 2014) and thus in this study a percentage TEC deviation of ± 45% was adopted (e.g. Dugassa et al. 2020). Monthly median values (e.g. Rishbeth 1963; Mendillo et al. 1974; Matamba et al. 2015), a number of quiet days before and after the main phase of a geomagnetic storm (e.g. Amabayo and Cilliers 2013), five internationally quietest days (e.g. Ikubanni et al. 2018), seven day median value (e.g. Astafyeva et al. 2015), or the quiet day before SSC (e.g. Kikuchi et al. 2008; Liu et al. 2016; Omojola and Adewumi 2020) were previously used as background values to remove the quiet-time background variation. In this analysis, the monthly median TEC values for the month within which the storm occurred were used as the background data to identify ionospheric storm effects. Hence, ionospheric storm effects were analysed using the equation:

$$\Delta TEC = \frac{TEC - TEC_m}{TEC_m} \times 100\%, \tag{1}$$

where ΔTEC is the percentage TEC deviation, and TEC_m is monthly median TEC value at a particular epoch.

The symmetric horizontal component of the ring current (SYM-H) (https://omniweb.gsfc.nasa.gov) was used to identify the onset of the geomagnetic storm. The SYM-H is similar to high-resolution disturbance storm-time (Dst) index (Iyemori 1990; Sugiura and Kamei 1991; Iyemori and Rao 1996) which describes the change in strength of the Earth's magnetic field (Dungey 1961; Sugiura 1963). Solar wind parameters were obtained from the National Aeronautics Space Administration (NASA) website (https://omniweb.gsfc.nasa.gov/). They included: solar wind speed (V_{SW}, km/s), IMF B_z (nT), and the solar wind dynamic pressure (P_{sw}, nPa). The interplanetary electric field (IEF) data was computed using the relation $\mathrm{IEF}_y = -v_{sw} \times Bz$ (Kelley 1989) and converted to mV/m by dividing it by 1000. The equatorial electric field (EEF) data was downloaded from PPEF model website (http://geomag.org/models/PPEFM/RealtimeEF.html). The PPEF model was developed by Manoj et al. (2008) using ionospheric drift measurements from the low-latitude JULIA (Jicamarca Unattended Long-term Investigations of the Ionosphere and Atmosphere) radar, and solar wind and IMF data from the ACE (Advanced Composition Explorer) satellite. To reduce on the discrepancy between the Scherliess–Fejer (S–F) climatological model (Scherliess and Fejer 1999) and the measured EEF, Manoj et al. (2008) proposed a transfer function between IEF and EEF. The S–F climatological model was developed using the incoherent scatter radar (ISR) observations at Jicamarca and Ion Drift Meter observations on board the Atmospheric Explorer E (AE-E) satellite (Scherliess and Fejer 1999). The S–F model is used in the PPEF model to account for the quiet day variations of EEF (Manoj et al. 2008). The transfer function was validated on synthetic as well as observed IEF data. It was found that the use of the transfer function increased the accuracy between IEF and EEF by 27% (Manoj et al. 2008; Manoj and Maus 2012). The vertical drift provided by the S–F climatological model is converted to the equatorial ionospheric eastward electric field by multiplying it with the magnetic field strength along the dip equator determined from the Challenging Mini-Satellite Payload (CHAMP) satellite data (Lühr et al. 2004).

The ionospheric current disturbances during the strong and severe geomagnetic storms that occurred on St. Patrick's day in 2013 and 2015 respectively were analysed using ground-based magnetometer data over Addis

Ababa (AAE) and Mbour (MBO) respectively. The AAE magnetometer station had no data in 2015. Near the equator, the orientation of the ionospheric electric currents is eastward in a horizontal direction which has a relationship with the eastward electric field (Grodji et al. 2017; Kashcheyev et al. 2018). According to Ohm's law, ionospheric currents lead to a deviation of the horizontal component of the Earth's magnetic field, H in the northward direction (Kashcheyev et al. 2018). Hence, the signature of ionospheric currents is the same and may be depicted by any magnetometer station along the equatorial region. In relation to this, data from MBO in Senegal was used during the ionospheric currents analysis in 2015. The magnetometer data used in this study were obtained from International Real-time Magnetic Observatory Network (INTERMAGNET) website (https://www.intermagnet.org/). The H component is expressed in terms of the north (X) and east (Y) components using the relation:

$$H = \sqrt{X^2 + Y^2}. \tag{2}$$

Since H combines all effects of the current systems within the magnetosphere–ionosphere system, it can be expressed as (Cole 1966; Fukushima and Kamide 1973; Amory-Mazaudier et al. 2017):

$$H_{\text{obs}} = S_R + D_{\text{iono}} + D_R + D_{CF} + D_T + D_G, \tag{3}$$

where S_R is the daily solar regular variation of the Earth's magnetic field estimated as the mean arithmetical value of H at each station for the five internationally quietest days of the month when the storm occurred, D_{iono} is the magnetic disturbance associated with the disturbed ionospheric current systems, D_R is the ring current, D_{CF} is Chapman–Ferraro current, D_T is the tail current, and D_G is due to magnetotelluric inducting currents. The strongest current is D_R which is expressed as:

$$D_R = \text{SYM-H} \cos\lambda, \tag{4}$$

where λ is the geomagnetic latitude of the station under consideration. When the contributing effects of the minimal current systems are neglected, Equation (3) becomes:

$$H_{\text{obs}} = S_R + D_{\text{iono}} + \text{SYM-H} \cos\lambda. \tag{5}$$

Hence, D_{iono} can be computed since the other components are readily available. The PPEF is subdivided into convection electric field and overshielding electric field (e.g Fejer 1986; Bagiya et al. 2017). In most cases, the former occurs mostly during main phase of the storm whilst the latter occurs during recovery phase of the storm (Kikuchi et al. 2008). The D_{iono} can be expressed as the sum of the polar disturbance equivalent current system related to PPEF (DP2) and the magnetic disturbance associated with DDEF (D_{dyn}) (Blanc and Richmond 1980; Nava et al. 2016; Amory-Mazaudier et al. 2017; Dugassa et al. 2020). The DP2 and D_{dyn} signals can be extracted from D_{iono} using a high-pass and a band-pass filter, respectively (Fathy et al. 2014; Nava et al. 2016; Azzouzi et al. 2015; Amory-Mazaudier et al. 2017; Amaechi et al. 2018; Dugassa et al. 2020; Matamba and Habarulema 2021). In this study, we used a band-pass filter to separate D_{dyn} from DP2 currents. The band-pass filter used to compute D_{dyn} was a moving average filter over 4 h period with a sliding window of 1 h (Fathy et al. 2014; Azzouzi et al. 2015), after which DP2 was calculated by subtracting D_{dyn} from D_{iono}. Table 1 shows the stations used in this study.

We checked the effect of composition changes during the study period using the $[O]/[N_2]$ ratio from the Global Ultra Violet Imager (GUVI) instrument onboard the Thermosphere Ionosphere Mesosphere Energetics and Dynamics (TIMED) satellite. The GUVI $[O]/[N_2]$ maps were obtained from the image gallery on the website: http://guvi.jhuapl.edu/site/gallery/guvi-galleryl3on2.shtml.

Table 1 Data stations used in this study

Station	Code	Geographic coordinates		Geomagnetic latitude
		Longitude	Latitude	
TEC data				
Addis Ababa	ADIS	38.8	9.0	0.2
Mbarara	MBAR	30.7	-0.6	-10.2
Magnetomer data				
Addis Ababa	AAE	38.8	9.0	0.2
Mbour	MBO	-17.0	14.4	2.1

Results and Discussion

In this section, the responses of the East African equatorial and low-latitude ionospheric region to 17 March 2013 and 17 March 2015 are presented. The possible mechanisms for the observed ionospheric TEC deviation are also presented. The two storms were categorised as strong and severe, respectively following the classification by Loewe and Prölss (1997).

16–18 March 2013 geomagnetic storm period

On 15 March 2013 at around 0600 UT, NASA reported an eruption of a magnetic filament snaking around sunspot AR1692 which produced an M1-class solar flare and a bright CME that was heading directly towards the Earth at a speed of 900 km/s (https://spaceweather.com/archive.php?view=1%20&day=17%20&month=

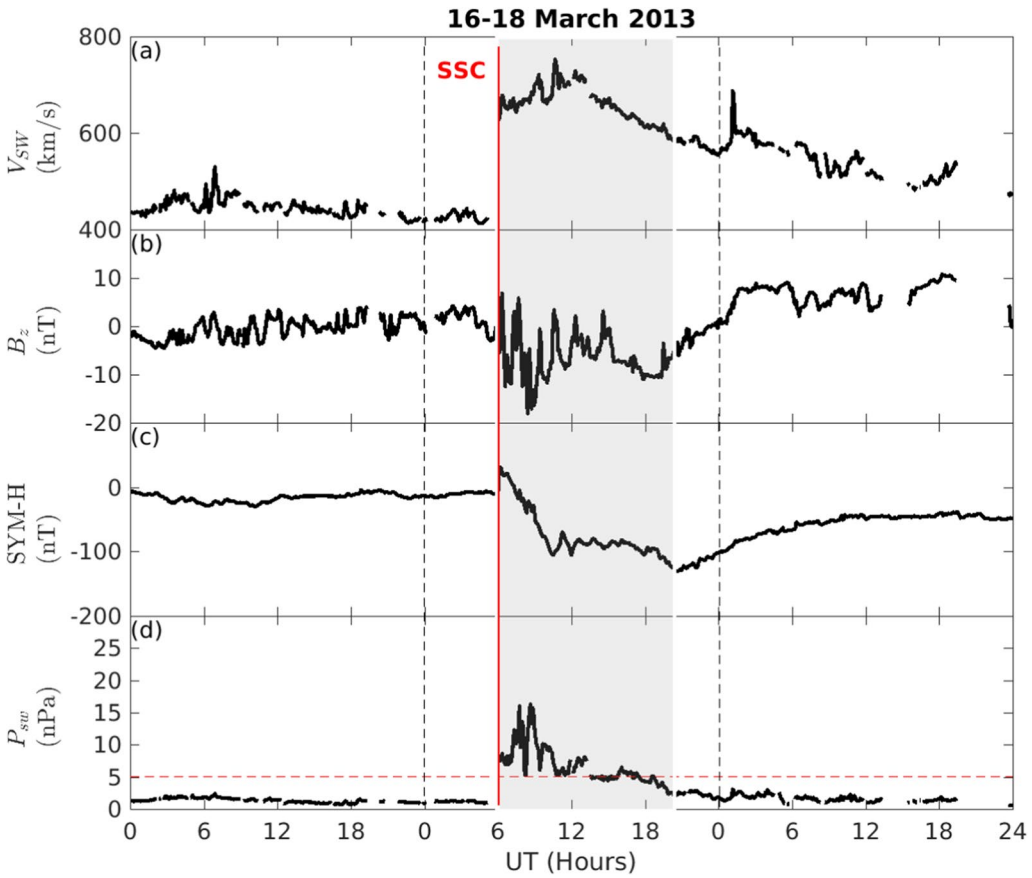

Fig. 1 Solar wind parameters for a strong geomagnetic storm that occurred between 16 and 18 March 2013. Panels present variations of (**a**) solar wind speed, V_{SW} (km/s), (**b**) z component of interplanetary magnetic field, IMF *Bz* (nT), (**c**) SYM-H (nT) and (**d**) solar wind pressure, P_{sw} (nPa) with time. The grey shaded region represents the main phase of the geomagnetic storm. The dotted red line represents the threshold value for P_{sw}.

03%20&year=2013). The CME hit the Earth's magnetic field at 0600 UT on 17 March 2013. The impact lifted the solar wind speed from 300 km/s to 700 km/s and sparked a strong geomagnetic storm. This storm had a minimum Dst index of -131 nT and a maximum kp index of 6 at 2100 UT (Yue et al. 2016; Omojola and Adewumi 2020). Figure 1 presents the geomagnetic storm evolution by considering a day before and after the storm main phase. Panels present V_{SW}, IMF *Bz* in Geocentric Solar Magnetospheric (GSM) coordinates, SYM-H, and P_{sw} for the storm period between 16 and 18 March 2013. The grey shaded region represents the main phase of the geomagnetic storm.

As seen in Fig. 1, the solar wind shock (SSC shown by solid red vertical line) arrived at about 0600 UT when the IMF *Bz* fluctuation amplitude varied significantly to about -20 nT and V_{SW} increased sharply (Fig. 1a, b). The IMF *Bz* remained southward and the SYM-H reached a minimum value of -131 nT at about 2025 UT (Fig. 1c). Due to the solar wind shock, an increase in the ground magnetic field was evident as seen in the abrupt increase in SYM-H at 0600 UT. The dotted red line on Fig. 1 (d) represents the threshold value for P_{sw} which is 5 nPa. The P_{sw} was above 5 nPa for over 8 h during the storm main phase. Hajra and Chakraborty (2011) asserted that local time (LT) of arrival and sustenance of magnetospheric shock compression ($P_{sw} > 5$ nPa) for a period greater than 6 h during local sunset-to-post sunset period may be treated as important precursor for penetration of eastward electric field to the equatorial and low-latitude zone. Thus, any ionospheric effects arising from the strong geomagnetic storm of 16–18 March 2013 during the time when $P_{sw} > 5$ nPa may be attributed to PPEF of the magnetospheric origin combined with the equatorward neutral wind.

16–18 March 2015 geomagnetic storm period

This storm occurred in the declining phase of solar cycle 24 and was the largest during this solar cycle. The storm was driven by interacting CMEs of 15 March 2015 (Liu et al. 2016) which began with a bang as reported by NASA. Between 0045 UT and 0200 UT, a magnetic

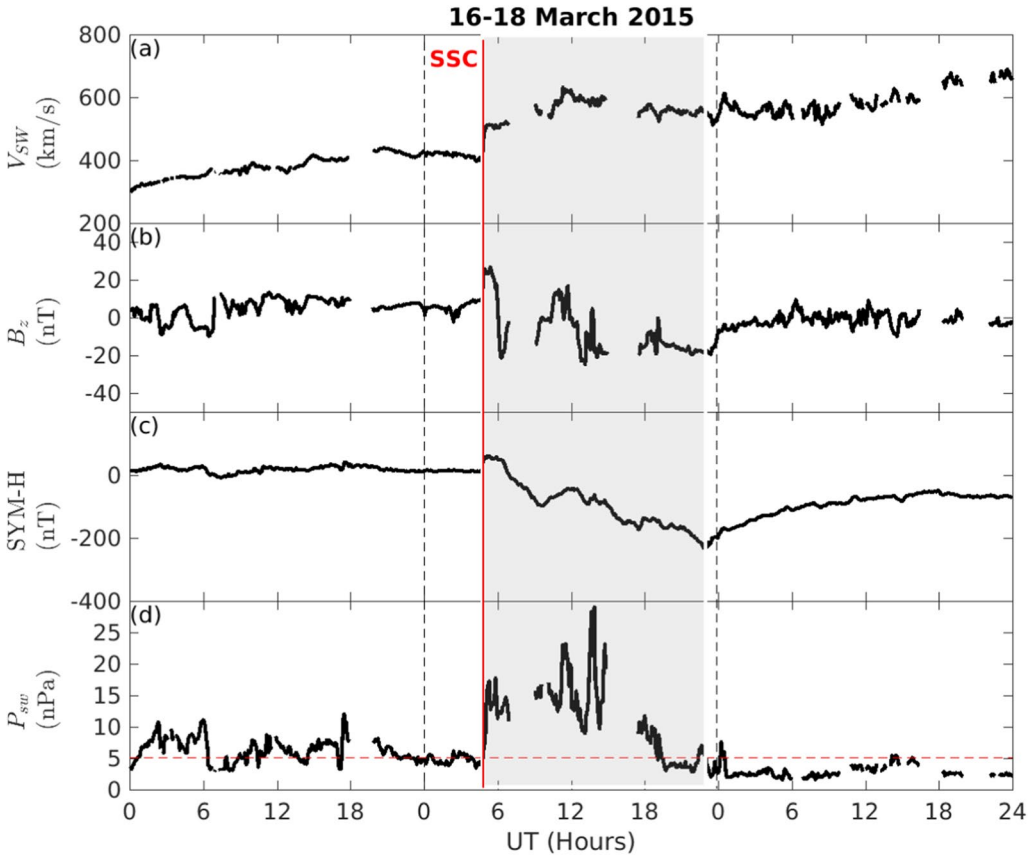

Fig. 2 Same as Fig. 1 but for a severe geomagnetic storm that occurred between 16–18 March 2015

filament erupted in concert with a slow C9-class solar flare from sunspot AR2297. The CME hit the Earth's magnetic field on 17 March 2015 at approximately 0430 UT. At first, the impact sparked a relatively mild G1-class (kp=5) geomagnetic storm. However, the storm intensified to G4-class (kp=8), ranking it as the severe geomagnetic storm during this solar cycle.

Figure 2 shows V_{SW}, IMF *Bz* in GSM coordinates, SYM-H and P_{sw} during 16–18 March 2015. The shaded area corresponds to the interval of the main phase of the storm. During the quiet day on 16 March 2015, the IMF *Bz* was mostly northward and the magnetic activity was weak on this day as depicted by SYM-H. The IMF *Bz* turned southward and reached a minimum value of -21 nT at 0615 UT. We notice that the P_{sw} was above 5 nPa even though the day was quiet. According to Hajra and Chakraborty (2011), one would expect PPEF during such conditions of P_{sw}. However, P_{sw} is highly dependent on the southward IMF *Bz* during the main phase of a storm (e.g. Adebesin et al. 2012). On 17 March 2015, when the interplanetary shock reached the magnetosphere, V_{SW} increased abruptly from 300 km/s to about 430 km/s during the day and P_{sw} was mostly above 5 nPa. The sharp increase of P_{sw} from $\sim$ 8 nPa to $\sim$ 30 nPa triggered an SSC as indicated by the step-like increase in SYM-H. For this storm, the magnetospheric shock compression ($P_{sw} > 5$ nPa) was sustained for a period of over 14 h during local sunset-to-post-sunset period. This also indicates that PPEF of the magnetospheric origin and equatorward neutral wind might have played a role on the observed ionospheric effects arising from this geomagnetic storm. The SSC occurred on 17 March 2015 at 0445 UT as indicated by the solid red vertical line. The storm reached a minimum value of the SYM-H of -233 nT at 2250 UT on the same day of SSC, after which it began the recovery phase through 18 March 2015. After the main phase, which ended at about 0000 UT on 18 March 2015, IMF *Bz* oscillated with a magnitude of around 5 nT. The V_{SW} kept relatively large values ranging from 450 km/s to 700 km/s and IMF *Bz* fluctuated between northward and southward. After this time, V_{SW} remained large but P_{sw} returned to its quiet-time level.

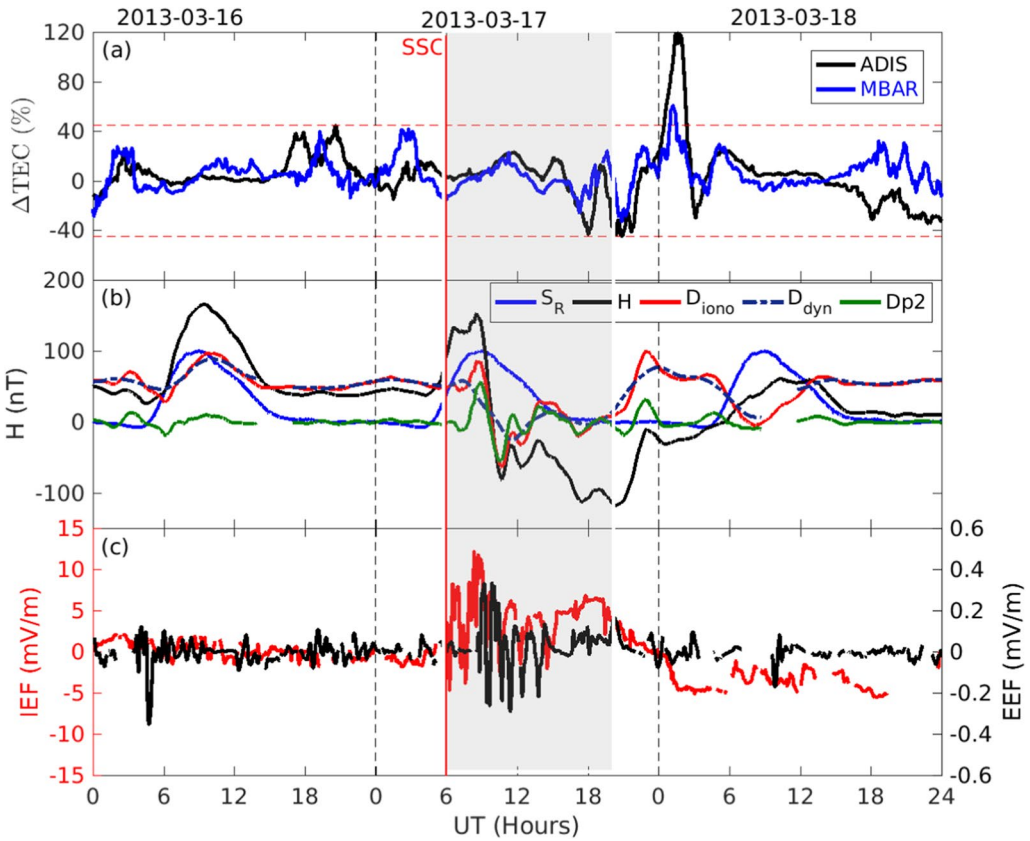

Fig. 3 Temporal variation of ionospheric characteristics, currents and electric fields during the strong geomagnetic storm of 16–18 March 2013

Ionospheric response, currents and electric fields during the strong storm of 16–18 March 2013

Figure 3 (a) presents ΔTEC (%) for the storm of 16–18 March 2013 over ADIS (black) and MBAR (blue). The dotted red line represents the threshold value of ΔTEC which is ± 45%.

Before the storm onset, on 16 March 2013, ΔTEC over ADIS was almost equal in magnitude to that over MBAR. There was no significant TEC deviation depicted from both stations during the main phase of the geomagnetic storm. During this strong geomagnetic storm, the ionosphere over MBAR did not show any significant response during the storm main phase. This is because transport process did not influence the distribution of plasma along the magnetic field lines, and thus no significant change in TEC during the storm main phase was observed. During the recovery phase of this storm, on 18 March 2013, ΔTEC was positive between 0000 UT and about 0300 UT over the two stations. This effect started to become significant at 0028 UT (0328 LT) and peaked at 0133 UT (0433 LT). This observation is in agreement with the findings of Buresova et al. (2012). During their analysis, the authors asserted that although the recovery phase would be characterised by an abatement of deviations and a gradual return to the quiet ionosphere, significant departures from the climatology may arise from the stormy ionosphere. The positive storm effect during the recovery phase (between 0000 UT and 0300 UT) may be attributed to equatorward neutral wind and strong DDEF which was eastward during the night depicted by D_{dyn} in Fig. 3 (b). The fact that equatorward neutral wind and DDEF contributed to plasma upward motion corroborates that electron density was at altitudes of lower diffusion and recombination rates such as in F2 region (e.g. Kelley 1989; Friedrich et al. 2004; Fagundes et al. 2016). In general, during the March 2013 geomagnetic storm the ionosphere over the trough of the East African region did not depict any significant TEC deviation during the storm main phase. A positive ionospheric effect was evident during the recovery phase of this storm for a duration of 55 min. The positive storm effect during the recovery phase may be attributed to equatorward neutral wind and D_{dyn} which exceeded DP2 current during this time (e.g. Biondi 1969; Fuller-Rowell et al. 1994; Ren et al. 2020). In addition, since transport process did not influence the distribution of plasma along the magnetic field lines (e.g. Kelley 1989), there was no significant change in TEC during the storm main phase. The main phase of

this storm coincided with the local morning hours when ionisation of the plasma was still at its minimum. This resulted in no appreciable changes in TEC. Shreedevi and Choudhary (2017) observed a positive ionospheric storm effect over the Indian sector during this very storm where the onset time of this storm coincided with the local noon in India. They found that the magnitude of the increase in TEC decreased northward of the dip equator and there was no appreciable change near the anomaly crest. They attributed the enhancement in TEC to photoproduction of ions. In this study, a minimum value of ΔTEC was attained during the main phase of the storm at 1800 LT over the trough of the East African region. For the same storm, Shreedevi and Choudhary (2017) observed a very sharp decrease in TEC magnitude after 1400 LT over the Indian anomaly region. The difference in the time of the minimum TEC between their study and this current one is due to the longitudinal differences between the two regions.

To study the effect of geomagnetic storms on the variation of the ionospheric currents during the 16–18 March 2013 geomagnetic storm, magnetometer data over AAE was used. The low-latitude ionospheric plasma significantly deviates from its quiet day's pattern under the effects of varying storm-time disturbance electric fields (PPEF and DDEF). Figure 3(b) presents the temporal variation in H, S_R, D_{iono}, D_{dyn} and DP2 during strong geomagnetic storm that occurred on 16–18 March 2013. Regular variations in ionospheric currents were observed during geomagnetically quiet days before and after the storm. However, on the day of the storm main phase (17 March 2013), fluctuations in the ionospheric currents were evident. The D_{iono} and D_{dyn} were close to each other implying that D_{dyn} which is as a result of DDEF contributed significantly to D_{iono}. During the main phase of the storm, between 0600 UT and 1200 UT, DP2 current was high compared to the previous day of 16 March 2013. On 17 March 2013, starting at 0600 UT, D_{dyn} was slightly higher than DP2. This basically explains the reason why there were no significant TEC changes during the main phase of the storm. During the recovery phase of the storm, there was no significant/minimal effect of DP2 currents to the ionospheric disturbances. We note that from Fig. 3 when D_{dyn} is westward, then DP2 is eastward. The net result is a bit of cancellation of the contributions from the two currents and the ionosphere may not show any major changes during storms. From Fig. 1(b), the polarity of IMF Bz was northward at

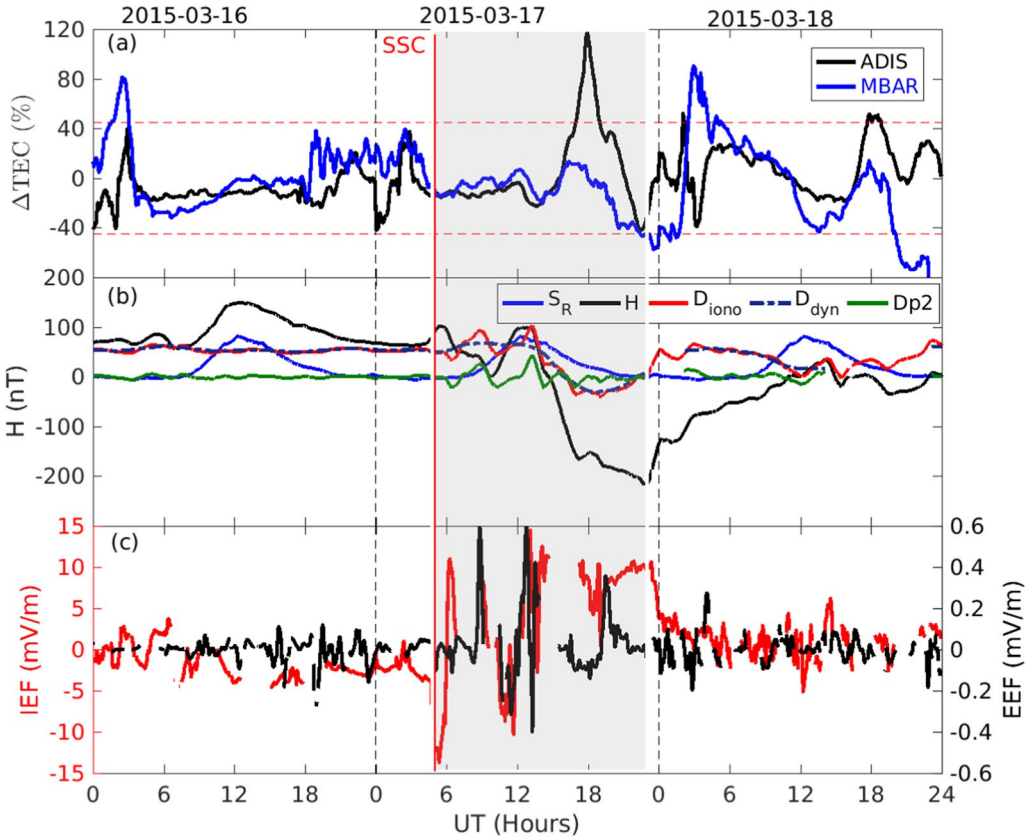

Fig. 4 Same as Fig. 3 but for a severe geomagnetic storm of 16–18 March 2015

0600 UT and this translates into the induction of westward electric field or reduction of eastward electric field. When IMF Bz turns southward, PPEF is observed but, in this case, probably it was small to effectively counteract the already existing DDEF resulting into no significant ionospheric changes (e.g. Tulasi Ram et al. 2019; Kumar et al. 2020). Figure 3(c) shows the diurnal variation of IEF and EEF during St. Patrick's day geomagnetic storm of 16–18 March 2013. The EEF was obtained from the PPEF model (Manoj et al. 2008). The IEF and EEF were able to capture the signatures of the geomagnetic storm as demonstrated by the increase in their amplitudes during the main phase of the storm. However, the changes of EEF during the main phase of the geomagnetic storm did not cause any significant change in ΔTEC. The fluctuations in EEF were more significant during the local daytime on the day of the storm (between 0900 UT and 1400 UT) whilst the D_{dyn} was at first eastward and changed the polarity to westward at around 1000 UT. Thus, the probable reason why there was no significant change in ΔTEC is the presence of the westward DDEF during the daytime which might have suppressed the DP2 current during the storm. Possibly, the D_{dyn} currents exceeded the DP2 currents resulting into a strong DDEF effect during the day than the PPEF effect. This means that the development of equatorial ionisation anomaly (EIA) was inhibited and thus no positive storm effect could be registered at the crest region (e.g. Simi et al. 2013; Luo et al. 2017; de Lourdes González 2022).

Ionospheric response, currents and electric fields during the severe storm of 16–18 March 2015

Figure 4(a) presents the effect of this geomagnetic storm on the ionosphere over ADIS (black curve) and MBAR (red curve). On 16 March 2015, between 0000 UT and 0600 UT, an enhancement in ΔTEC was evident over MBAR and reached a maximum value of ∼ 80 TECU. This enhancement may be attributed to pre-storm effects over the low-latitude region (e.g. Nogueira et al. 2011; Danilov 2013; Picanço et al. 2021). The ionosphere over ADIS showed a positive response to this geomagnetic storm during the main phase. The ionosphere over MBAR did not show any significant response to this geomagnetic storm during the main phase, but a positive storm effect was observed during the storm recovery phase on 18 March 2015.

We further investigated the influence of ionospheric currents on the ionosphere over East Africa as a result of the geomagnetic storm of 16–18 March 2015 using the magnetometer data. It should be noted that over the East African region, there was no magnetometer data during the geomagnetic storm of 16–18 March 2015. We therefore used data over MBO to carry out this investigation. The LT difference between MBO and ADIS is about 3 h. The data over MBO was used because the magnetic variations and hence the ionospheric currents over the same latitude region are expected to be the same (Grodji et al. 2017; Kashcheyev et al. 2018). Besides, H component of the Earth's magnetic field exhibits common patterns during a geomagnetic storm in all sectors at the same universal time (UT) (Nava et al. 2016). Small differences, attributed to LT effects, normally exist during the first hours of the storm main phase. From Fig. 4(b), H deviated from S_R with a minimum value of above − 200 nT compared to − 100 nT in Fig. 3(b). This may be attributed to the difference in the intensities of the two storms. Nevertheless, D_{iono} and D_{dyn} followed the same trend except during the main phase of the storm where fluctuations in D_{iono} were observed. During the geomagnetically quiet day on 16 March 2015, DP2 was undisturbed. The fluctuations in DP2 maximised on 17 March 2015 at 1310 UT (1310 LT) and this may be attributed to PPEF of the magnetospheric origin since IMF *Bz* was southward during this time (e.g. Liu et al. 2014; Amaechi et al. 2020). The existence of equatorward neutral wind and PPEF during local daytime leads to increased vertical $\mathbf{E} \times \mathbf{B}$ drift and thus development of EIA whilst DDEF during local daytime can lead to suppression of EIA (Liu et al. 2014; Yadav et al. 2016). The positive storm effect depicted by ΔTEC over ADIS in Fig. 4(a) with a maximum value of 120 TECU at 1758 UT (2058 LT) may be attributed to the effects of DDEF which was westward during this time as depicted by D_{dyn}, whilst DP2 was close to the quiet-time level. This positive effect started to become significant at 1703 UT (2003 LT) and thus took 55 min to maximise. Nava et al. (2016) observed simultaneous oscillations of the Earth's magnetic field in the Asian, African and American sectors due to southward magnetisation of IMF *Bz*. The positive ionospheric storm effect over MBAR during the recovery phase of the storm, between about 0300 UT (0600 LT) and 0400 UT (0700 LT) may be attributed to the strong eastward DDEF depicted by D_{dyn}. This implies that the electron density was at high altitudes where recombination rate is low. We noticed an increase in TEC near the crest on the days before and after the storm, and at the trough during the main phase of the storm. In all longitudinal sectors, Nava et al. (2016) observed an increase in TEC at the beginning of the storm which was evident at the crests of the equatorial anomaly, followed by a decrease in TEC at the mid- and high-latitudes. We observed a negative storm effect immediately after the storm main phase, whose cause would not be attributed to any ionospheric current due to the data gap. During their analysis, Nava et al. (2016) observed no increase

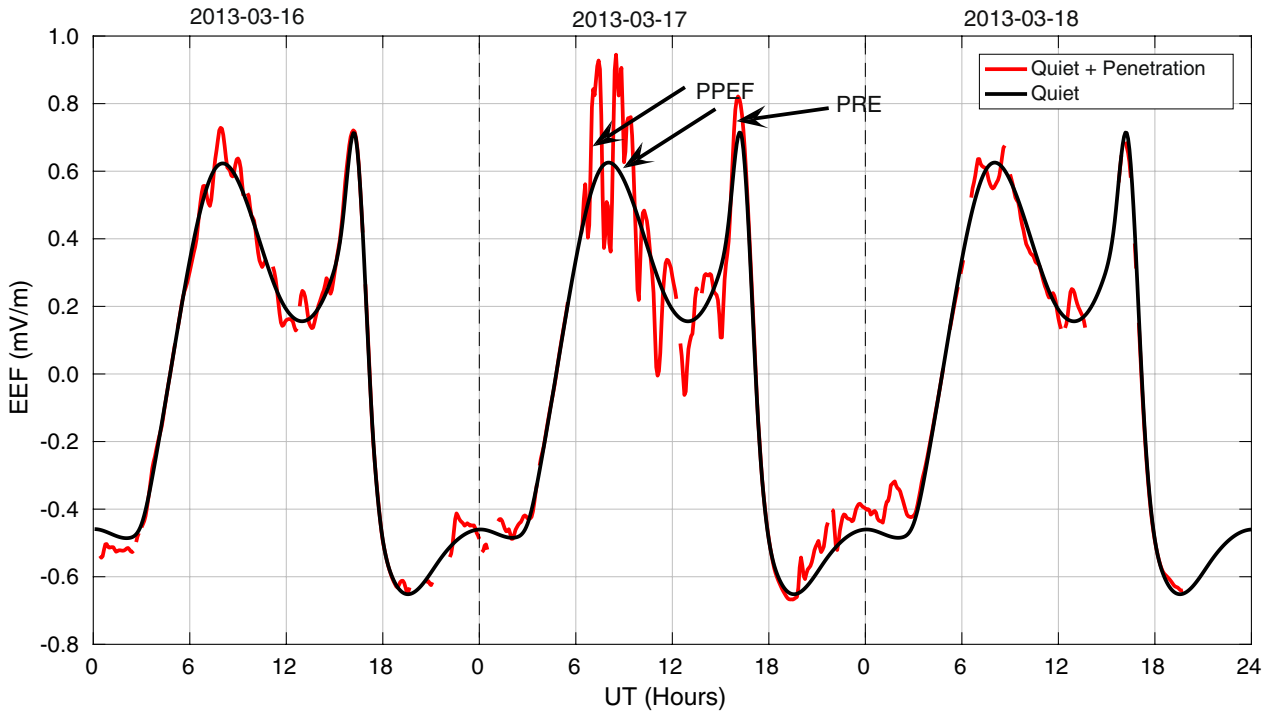

Fig. 5 Effect of penetration electric field on the quiet-time EEF during the geomagnetic storm of 16–18 March 2013

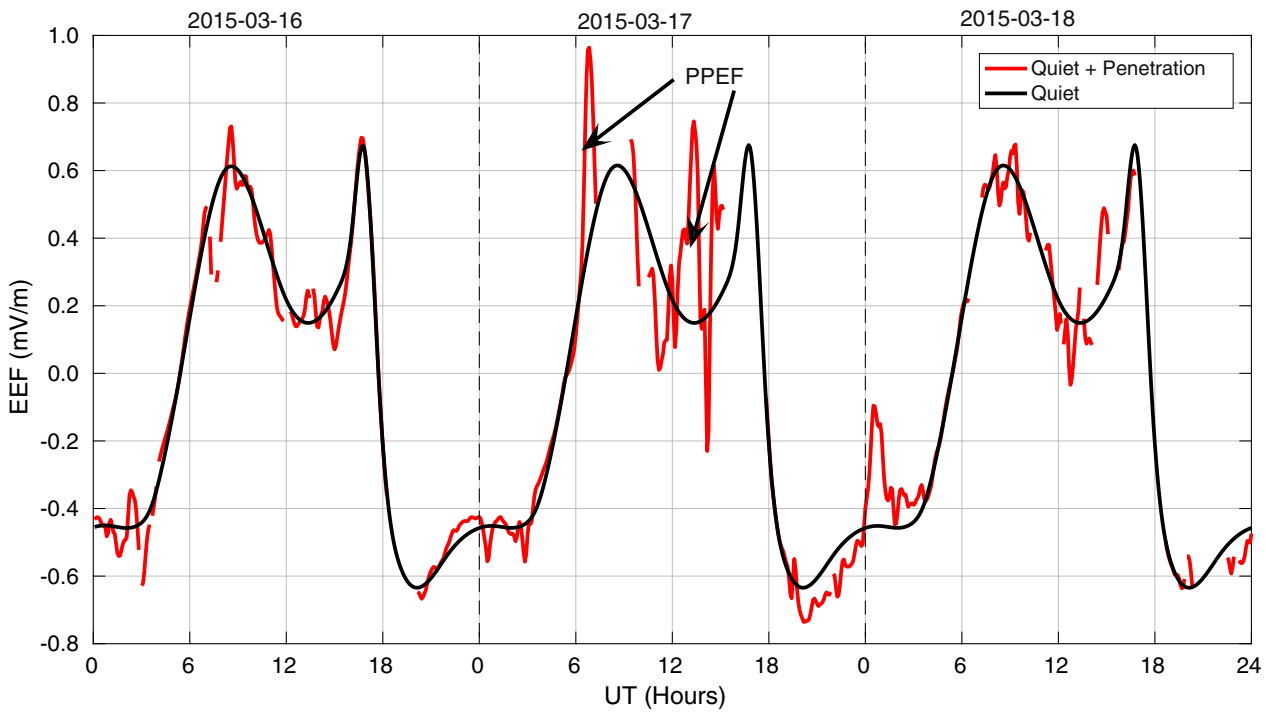

Fig. 6 Same as Fig. 5 but for the geomagnetic storm of 16–18 March 2015

in TEC during the storm day but rather a decrease in TEC over MBAR (southern low-latitude) during the early hours of the recovery phase of the storm. In our analysis, a positive storm effect was observed over ADIS which also lies within the equatorial region. During the storm main phase, the magnitude of the IEF and EEF increased significantly from their quiet-time values during the day before and after the geomagnetic storm as shown on Fig. 4(c). This value was greater than the one in Fig. 3(c) by about 5 mV/m, possibly due to the difference in intensities of the two geomagnetic storms.

To verify whether PPEF was the main driver of ionospheric response during the main phases of the two geomagnetic storms, the EEF data for the two storms was plotted as a function of UT (UT = LT − 3) over ADIS. Figure 5 shows the combined PPEF and quiet EEF (in red) superimposed on the quiet EEF only (in black). The quiet-time pattern of EEF is smooth and uniform. The superposed effect of both the quiet-time and penetration electric field, on the other hand, shows fluctuations and as a result there were cases where the penetration electric field was above or below the quiet-time EEF.

Quiet EEF was obtained using the EEF data for the five quietest days in a month in which the storm occurred. The quietest days of the month were obtained from GFZ Helmholtz Potsdam Centre in Germany (https://dataservices.gfz-potsdam.de/portal/) as March 8, 7, 26, 25 and 13 in 2013 and March 10, 30, 5, 14 and 9 in 2015. This implies that the penetration effect can be visualised by subtracting the latter from the former. It can be observed from Fig. 5 that on the day prior to the storm (16 March 2013), penetration electric field was minimal at around 0700 UT. For the rest of the day, there was no PPEF, an indication that there was no magnetic activity, hence a quiet day. On 17 March 2013, two instances showing eastward PPEFs were evident at about 0700 UT (1000 LT) and 0900 UT (1200 LT), the time during which IMF *Bz* was southward. Even though there was a data gap on 18 March 2013, there seemed to be no instance of PPEF where data was available during the recovery phase of the storm.

Figure 6 is similar to Fig. 5 but for a storm that occurred on 17 March 2015. The magnitude of the penetration electric field during the 16–18 March 2015 geomagnetic storm was slightly higher than that of 16–18 March 2013. From Fig. 6, 16 March 2015 was quiet with no significant penetration electric fields. On 17 March 2015, PPEF existed at around 0600 UT (0900 LT) and 1200 UT (1500 LT). On 18 March 2015, there were instances of penetration electric field between 0000 UT (0300 LT) and 0200 UT (0500 LT). This dawn–dusk penetration electric field might have been responsible for ΔTEC enhancement during the recovery phase of the storm in Fig. 4(a). We may thus surmise that the ionospheric responses to geomagnetic storms of St. Patrick's days over the equatorial and low-latitude region of Africa were as a result of the combined effect of equatorward neutral wind, PPEF and DDEF. During the southward turnings of IMF *Bz* that took place at about 1435 UT (1735 LT) on 17 March 2013, eastward PPEF occurred in the post-sunset period starting at about 1600 UT (1900 LT) and enhanced the PRE (Fig. 5). The presence of westward PPEF at around 1500 UT acted to suppress the PRE on 17 March 2015 (Fig. 6).

Effect of composition changes on the observed ionospheric responses

To study the effect of composition changes on the observed ionospheric responses, we used the $[O]/[N_2]$ data from the Global Ultra Violet Imager (GUVI) instrument on-board the Thermosphere Ionosphere Mesosphere Energetics and Dynamics (TIMED) satellite. Observation of the day-to-day variation $[O]/[N_2]$ is feasible since the satellite traverses the same region nearly at the same time in consecutive days (Zhang et al. 2004; Tesema et al. 2015; Nava et al. 2016). Figure 7 presents the global map of thermospheric $[O]/[N_2]$ for the period between 16 and 18 March 2013, with each panel representing the 24 h of a day at a nearly constant local time of 1000 LT as the Earth rotates under the satellite orbit (e.g. Zhang et al. 2004; Nava et al. 2016). The white spaces in each panel on the maps represent the data gaps.

The pattern of $[O]/[N_2]$ between 16 and 18 March 2013 over the East African sector was checked. There were no appreciable changes in $[O]/[N_2]$ over this sector between 16 and 18 March 2013. This agrees with the observations in Fig. 3(a) especially at around 1000 UT when no obvious TEC increase is observed. The increase in TEC in Fig. 3(a) seems to be a nighttime feature and the $[O]/[N_2]$ data may not tell us what happened since the data is restricted to a particular LT (e.g. Zhang et al. 2004).

Figure 8 is the same as Fig. 7 but for the period between 16 and 18 March 2015. We observed a different pattern of $[O]/[N_2]$ between 16 and 18 March 2015 over the East African sector. In general there was an appreciable change in $[O]/[N_2]$ between 16 and 18 March 2015. The $[O]/[N_2]$ increase was more pronounced/obvious on 18 March 2015. The physical mechanisms relate to changes in thermospheric composition/composition bulge from high latitudes (Rishbeth 1991; Prölss 1995; Fuller-Rowell et al. 1994; Mendillo 2006; Tsagouri 2022). The results from the composition changes may not necessarily agree with interpretation of electric field contributions as one is dynamic whilst the other is electrodynamic (e.g. Rishbeth 1991; Prölss 1995; Fuller-Rowell et al. 1994). These

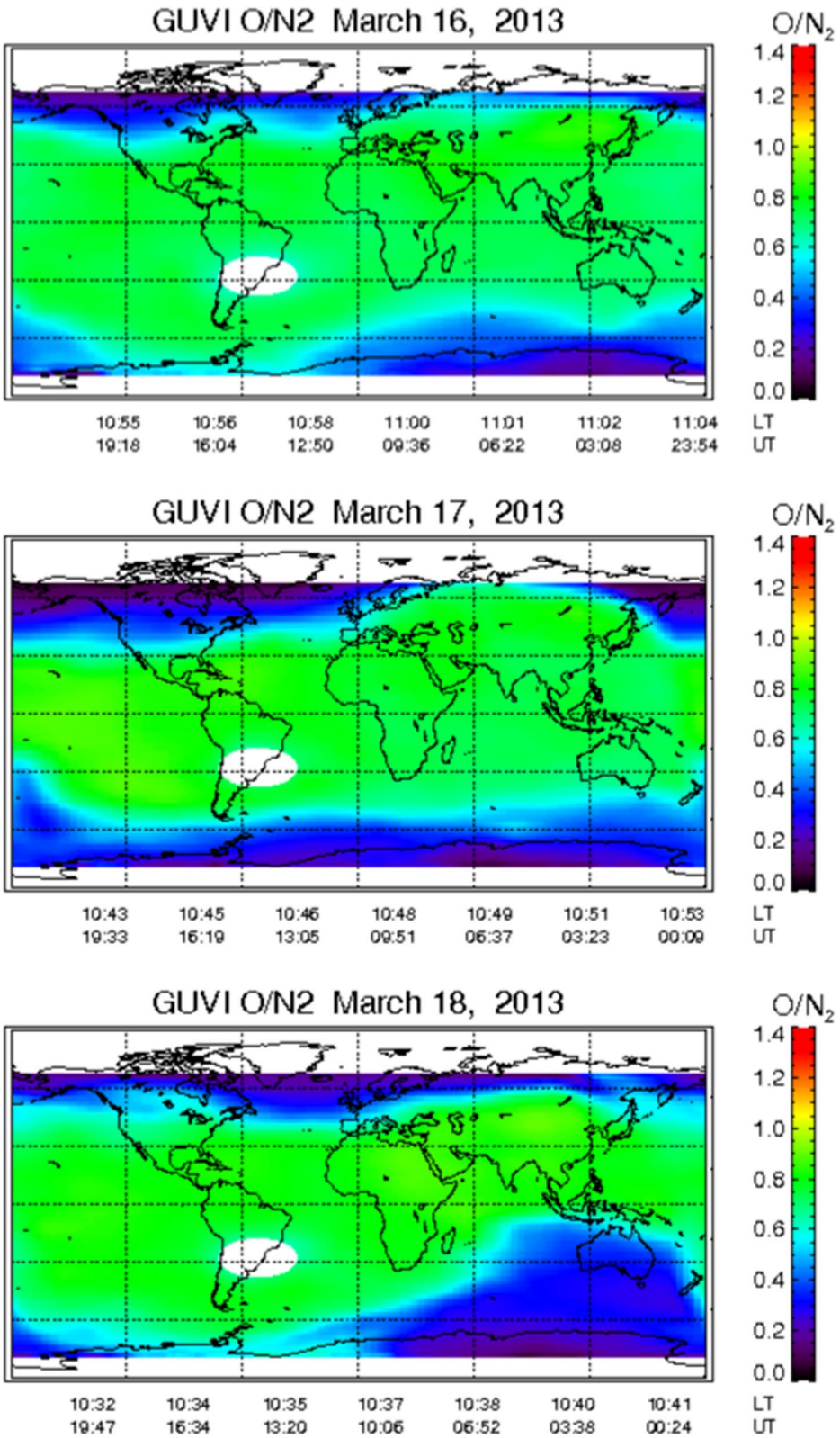

Fig. 7 Global map of thermospheric [O]/[N_2] from the Global Ultraviolet Imager (GUVI) experiment flown on the TIMED satellite for the period between 16 and 18 March 2013. Data gaps are represented by the white spaces in each panel

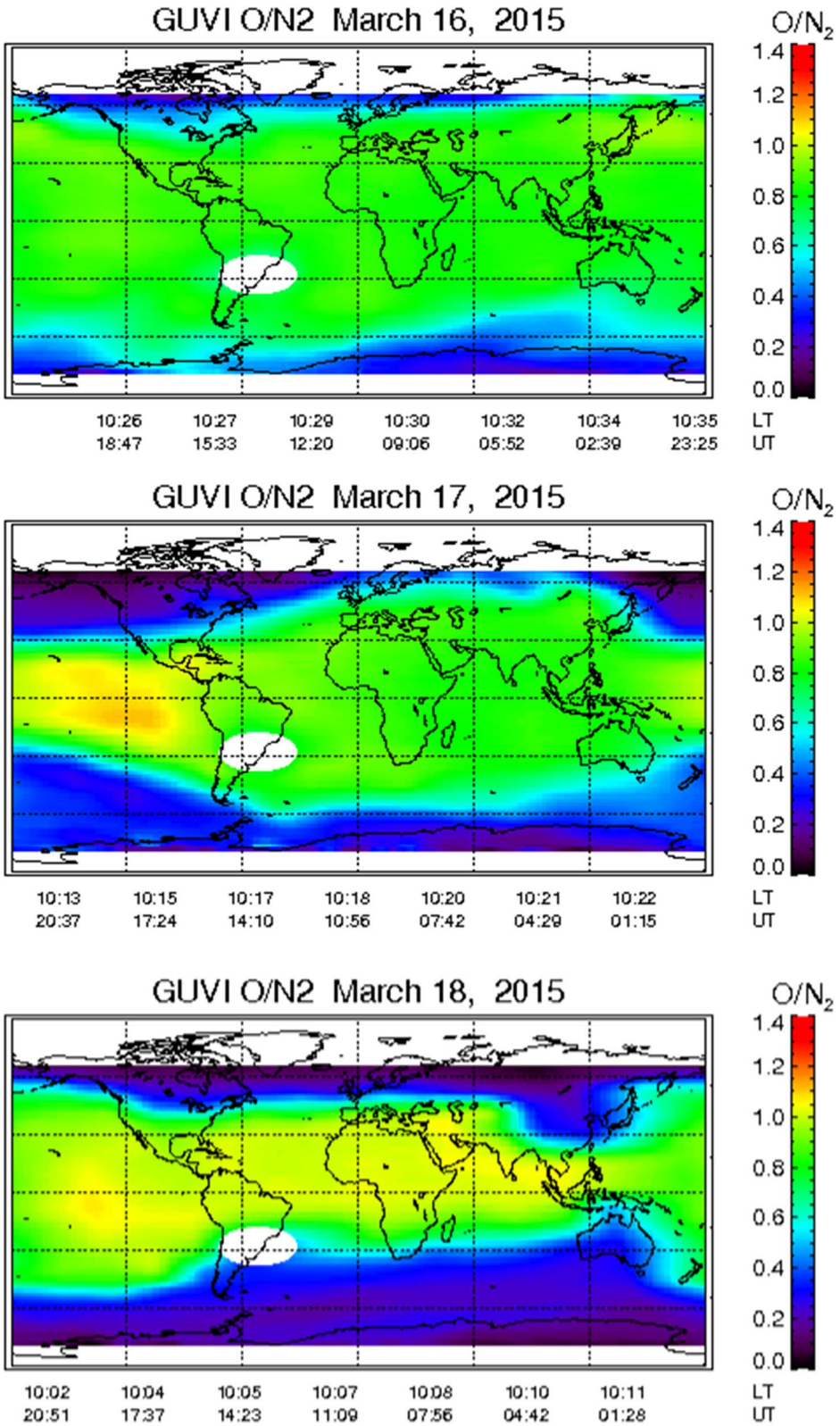

Fig. 8 Same as Fig. 7 but for the period between 16 and 18 March 2015

$[O]/[N_2]$ observations may not tell exactly the origin of the positive ionospheric storms in Fig. 4(a) because these ionospheric storms are nighttime features. Besides, positive ionospheric storms can not be conclusively attributed to composition changes in $[O]/[N_2]$ (e.g. Prölss 1995; Förster et al. 1999).

Similarities and differences between the two St. Patrick's day geomagnetic storms

To elucidate the driving mechanisms of the two St. Patrick's day geomagnetic storms, we describe the scientific similarities and/or differences between the two storms. Both storms occurred during the local daytime and in the same season (March equinox). However, 2013 was a solar maximum year whilst 2015 was the descending phase of solar cycle 24. In addition, 2013 (2015) storm was strong (severe). Both storms were as a result of CME. The day before the solar wind compressed the magnetosphere was quiet for both storms until when SSC was reached. The two storms depicted similar changes in V_{SW} with a shock of up to about 700 km/s and 500 km/s in 2013 and 2015 respectively on St. Patrick's day. Hence the two storms exhibited solar wind shocks with V_{SW} increasing to a value above 500 km/s accompanied by southward turning of the IMF *Bz* component to a value of about -20 nT which triggered the storm occurrences. In both cases, the variations in SYM-H are accompanied by the same variations in IMF *Bz*. The main phase of the two storms ended during post-sunset hours of the St. Patrick's day, with the one of March 2013 (2015) at (after) local midnight. It should be noted that after the SSC of 17 March 2013 (17 March 2015) which corresponded to the arrival of a CME on Earth's magnetosphere, an increase in P_{sw} was evident which reached a value above 15 nPa in both cases. The P_{sw} for both storms exceeded the threshold value of 5 nPa for a period of more than 6 h during the main phase. The behaviour of ΔTEC for the two storms exhibits different features due to the different durations of the main phase of the two storms. The March 2013 geomagnetic storm exhibited a shorter duration of the main phase than that of March 2015. The anti-Sq signature which is the fluctuation of D_{iono} with opposite sign to Sq was more prominent during the main phase of March 2013 than 2015 geomagnetic storm. For the two geomagnetic storms, there was a positive storm effect during the recovery phase attributed to strong DDEF which was eastward during the night depicted by D_{dyn}. In this study, we sought to identify the differences and/or similarities in ionospheric responses as a result of the storms which occurred on 17 March 2013 and 2015. The new result that we derive from this study is that there was a difference in the ionospheric response over the East African region yet these two storms occurred on the same day of the year but in different years.

Conclusions

In this study, simultaneous analysis of the effect of the two St. Patrick's day geomagnetic storms that occurred during the March 2013 and 2015 on the equatorial and low-latitude ionospheric region of Africa was carried using GPS-TEC data obtained from IGS stations, magnetometer data observations and real-time PPEF model. These were used to obtain the response of the ionosphere to geomagnetic storms using monthly median TEC data for the month within which the geomagnetic storm under consideration occurred as the measure of background variability in TEC. The response of the ionosphere to a geomagnetic storm was considered to be significant if $|\Delta\ \text{TEC}| \geq 45\%$. We found out that the ionosphere over the East African trough and crest regions did not show any significant response to the two St. Patrick's days geomagnetic storms during the main phase, except on 17 March 2015 over ADIS where a positive response was observed at 1800 UT. However, during the recovery phase, the ionosphere showed a positive response over the trough and crest regions of East Africa. For the storm that occurred on 17 March 2013 (17 March 2015), the magnetospheric shock compression ($P_{sw} > 5$ nPa) was sustained for a period of over 8 (14) hours during local sunset-to-post-sunset period, which may be treated as important precursor for penetration of eastward electric field to the equatorial and low-latitude zone (Hajra and Chakraborty 2011). This indicates that equatorward neutral wind and PPEF of the magnetospheric origin played a role on the observed ionospheric effects arising from the two St. Patrick's day geomagnetic storms. We further investigated the extent to which ionospheric currents influenced ionospheric variability during the geomagnetic storms. We found out that on the storm day of 17 March 2013 the fluctuations in the ionospheric current were evident with D_{dyn} contributing significantly to D_{iono}. H deviated much from S_R indicating that magnetospheric currents were modified by the storm occurrence. However, for the storm of 17 March 2015, H deviated from S_R with a minimum value of above − 200 nT compared to − 100 nT on 17 March 2013. This may be attributed to the difference in the intensities of the two storms. For the two geomagnetic storms, there was a positive storm effect during the recovery phase attributed to strong DDEF which was eastward during the night depicted by D_{dyn}. The pattern of $[O]/[N_2]$ between 16 and 18 March 2013 and 2015 over the East African sector was checked. There were no appreciable changes in $[O]/[N_2]$ over this sector between 16 and 18 March 2013. We observed a different pattern of $[O]/[N_2]$ between 16 and 18 March 2015 over the East African sector. In general, there was an appreciable change in $[O]/[N_2]$

between 16 and 18 March 2015. The $[O]/[N_2]$ increase was more pronounced/obvious on 18 March 2015. The physical mechanisms relate to changes in thermospheric composition/composition bulge from high latitudes (Rishbeth 1991; Prölss 1995; Fuller-Rowell et al. 1994; Mendillo 2006; Tsagouri 2022). We may thus surmise that the ionospheric responses to geomagnetic storms of St. Patrick's days over the equatorial and low-latitude region of East Africa were as a result of the combined effect of equatorward neutral wind, PPEF and DDEF.

Abbreviations

TEC	Total electron content
GNSS	Global Navigation Satellite System
ΔTEC	TEC deviation
IMF B_z	Z component of Interplanetary magnetic field
EEF	Equatorial electric field
PPEF	Prompt penetration electric field
PRE	Prereversal enhancement
DDEF	Disturbed dynamo electric field
CMEs	Coronal mass ejections
CIRs	Corotating interaction regions
SSC	Sudden storm commencement
HF	High frequency
TADs	Travelling atmospheric disturbances
TIDs	Travelling ionospheric disturbances
DMSP	Defense meteorological satellite program
C/NOFS	Communication/Navigation Outage Forecasting System
EPBs	Equatorial plasma bubbles
RINEX	Receiver INdependent EXchange
GPS	Global positioning system
VTEC	Vertical TEC
SYM-H	Symmetric horizontal component of the ring current
IEF	Interplanetary electric field
P_{sw}	Solar wind dynamic pressure
JULIA	Jicamarca Unattended Long-term Investigations of the Ionosphere and Atmosphere
ACE	Advanced Composition Explorer
ISR	Incoherent scatter radar
AE-E	Atmospheric Explorer E
CHAMP	Challenging Mini-Satellite Payload
INTERMAGNET	International Real-time Magnetic Observatory Network
GSM	Geocentric Solar Magnetospheric
LT	Local time
UT	Universal time

Acknowledgements
We acknowledge the provision of GPS-TEC analysis software developed at Boston College. The authors thank UNAVCO (https://data.unavco.org/archive/gnss/rinex/obs/) for the provision of RINEX data. The Interplanetary magnetic field, and the solar wind data were obtained on the website: https://omniweb.gsfc.nasa.gov/cgi/nx1.cgi. The symmetric horizontal component of the ring current (SYM-H) was obtained from https://omniweb.gsfc.nasa.gov/. The EEF data was obtained from the PPEF model on the website: http://geomag.org/models/PPEFM/RealtimeEF.html. We thank INTERMAGNET network (https://www.intermagnet.org/) for the provision of the magnetometer data used in this study. The Global thermospheric $[O]/[N_2]$ maps were downloaded from the website: http://guvitimed.jhuapl.edu/guvi-galleryl3on2.shtml.

Author contributions
VH, JBH and TD designed and conducted the current research and prepared the manuscript. VH analysed the RINEX data. TD analysed the magnetometer data and interpreted the results. JBH assisted in the interpretation of the results, and editing of the draft. All authors read and approved the final manuscript.

Availability of data and materials
The magnetometer data used is publicly available on https://www.intermagnet.org/. The RINEX data can be downloaded from https://data.unavco.org/archive/gnss/rinex/obs/. The solar wind data can be accessed on https://omniweb.gsfc.nasa.gov/cgi/nx1.cgi.

Declarations

Ethics approval and consent to participate
Not applicable.

Consent for publication
Not applicable.

Competing interests
The authors declare that they have no competing interests.

Author details
[1]Department of Physics, Mbarara University of Science and Technology, Mbarara, Uganda. [2]South African National Space Agency (SANSA) Space Science, 7200 Hermanus, South Africa/Department of Physics and Electronics, Rhodes University, Makhanda 6140, South Africa. [3]Entoto Observatory and Research Center, Addis Ababa, Ethiopia/Space Science and Geospatial Institute, Addis Ababa, Ethiopia.

Received: 29 August 2022 Accepted: 30 March 2023
Published online: 20 April 2023

References

Adebesin OB, Ikubanni OS, Kayode J (2012) Solar wind dynamic pressure dependency on the plasma flow speed and IMF Bz during different geomagnetic activities. World J Young Res 2(3):43–53
Amabayo EB, Cilliers JP (2013) Multi-station observation of ionospheric irregularities over South Africa during strong geomagnetic storms. Adv Space Res 51(5):754–771
Amabayo EB, McKinnell L-A, Cilliers JP (2012) Ionospheric response over South Africa to the geomagnetic storm of 11–13 April 2001. J Atmospheric Solar Terr Phys 84:62–74
Amabayo EB, Edward J, Cilliers PJ, Habarulema JB (2014) Climatology of ionospheric scintillations and TEC trend over the Ugandan region. Adv Space Res 53(5):734–743
Amaechi P, Oyeyemi E, Akala A (2018) Geomagnetic storm effects on the occurrences of ionospheric irregularities over the African equatorial/low-latitude region. Adv Space Res 61(8):2074–2090
Amaechi P, Oyeyemi E, Akala A, Amory-Mazaudier C (2020) Geomagnetic activity control of irregularities occurrences over the crests of the African EIA. Earth Space Sci 7(7):e2020EA001183
Amory-Mazaudier C, Bolaji O, Doumbia V (2017) On the historical origins of the CEJ, DP2, and Ddyn current systems and their roles in the predictions of ionospheric responses to geomagnetic storms at equatorial latitudes. J Geophys Res Space Phys 122(7):7827–7833
Astafyeva E, Zakharenkova I, Förster M (2015) Ionospheric response to the 2015 St. Patrick's Day storm: a global multi-instrumental overview. J Geophys Res Space Phys 120(10):9023–9037
Azzouzi I, Migoya-Orue Y, Mazaudier CA, Fleury R, Radicella SM, Touzani A (2015) Signatures of solar event at middle and low latitudes in the Europe-African sector, during geomagnetic storms, October 2013. Adv Space Res 56(9):2040–2055
Bagiya MS, Sunil A, Chakrabarty D, Sunda S (2017) Salient features of the dayside low latitude ionospheric response to the main phase step-I of the 17 March 2015 geomagnetic storm. Adv Space Res 60(8):1827–1837
Balan N, Shiokawa K, Otsuka Y, Watanabe S, Bailey G (2009) Super plasma fountain and equatorial ionization anomaly during penetration electric field. J Geophys Res Space Phys 114(3):114

Balan N, Shiokawa K, Otsuka Y, Kikuchi T, Vijaya Lekshmi D, Kawamura S, Yamamoto M, Bailey G (2010) A physical mechanism of positive ionospheric storms at low latitudes and midlatitudes. J Geophys Res Space Phys 115(2):112

Balan N, Otsuka Y, Nishioka M, Liu J, Bailey G (2013) Physical mechanisms of the ionospheric storms at equatorial and higher latitudes during the recovery phase of geomagnetic storms. J Geophys Res Space Phys 118(5):2660–2669

Basu S, Basu S, MacKenzie E, Bridgwood C, Valladares C, Groves K, Carrano C (2010) Specification of the occurrence of equatorial ionospheric scintillations during the main phase of large magnetic storms within solar cycle 23. Radio Sci 45(05):1–15

Biondi MA (1969) Atmospheric electron-ion and ion-ion recombination processes. Can J Chem 47(10):1711–1719

Blanc M, Richmond A (1980) The ionospheric disturbance dynamo. J Geophys Res Space Phys 85(A4):1669–1686

Borries C, Mahrous AM, Ellahouny NM, Badeke R (2016) Multiple ionospheric perturbations during the Saint Patrick's Day storm 2015 in the European-African sector. J Geophys Res Space Phys 121:333–345

Buresova D, Lastovicka J, Boska J, Sindelarova T, Chum J (2012) Ionospheric Behaviour During Storm Recovery Phase. EGU general assembly conference abstracts, Vienna

Cole K (1966) Magnetic storms and associated phenomena. Space Sci Rev 5(6):699–770

Danilov A (2013) Ionospheric F-region response to geomagnetic disturbances. Adv Space Res 52(3):343–366

Danilov A, Morozova L (1985) Ionospheric storms in the F2 region-morphology and physics. Geomagn Aeron 25:705–721

de Lourdes González G (2022) Ionospheric irregularities during disturbed geomagnetic conditions over argentinian EIA region. Acta Geodaetica Geophys 57:129–155

Dugassa T, Habarulema JB, Nigussie M (2019) Investigation of the relationship between the spatial gradient of total electron content (TEC) and the occurrence of ionospheric irregularities. Ann Geophys 37:1161–1180

Dugassa T, Habarulema JB, Nigussie M (2020) Equatorial and low-latitude ionospheric TEC response to CIR-driven geomagnetic storms at different longitude sectors. Adv Space Res 66(8):1947–1966

Dungey JW (1961) Interplanetary magnetic field and the auroral zones. Phys Rev Lett 6(2):47

Fagundes PR, Cardoso F, Fejer B, Venkatesh K, Ribeiro B, Pillat V (2016) Positive and negative GPS-TEC ionospheric storm effects during the extreme space weather event of March 2015 over the Brazilian sector. J Geophys Res Space Phys 121(6):5613–5625

Fathy I, Amory-Mazaudier C, Fathy A, Mahrous A, Yumoto K, Ghamry E (2014) Ionospheric disturbance dynamo associated to a coronal hole: Case study of 5–10 April 2010. J Geophys Res Space Phys 119(5):4120–4133

Fejer BG (1986) Equatorial ionospheric electric fields associated with magnetospheric disturbances. Solar Wind Magnetos Coupling 126:519

Feng J, Zhou Y, Zhou Y, Gao S, Zhou C, Tang Q, Liu Y (2021) Ionospheric response to the 17 March and 22 June 2015 geomagnetic storms over Wuhan region using GNSS-based tomographic technique. Adv Space Res 67(1):111–121

Förster M, Namgaladze A, Yurik RY (1999) Thermospheric composition changes deduced from geomagnetic storm modeling. Geophys Res Lett 26(16):2625–2628

Friedrich M, Torkar K, Steiner R (2004) Empirical recombination rates in the lower ionosphere. Adv Space Res 34(9):1937–1942

Fukushima N, Kamide Y (1973) Partial ring current models for worldwide geomagnetic disturbances. Rev Geophys 11(4):795–853

Fuller-Rowell T, Codrescu M, Moffett R, Quegan S (1994) Response of the thermosphere and ionosphere to geomagnetic storms. J Geophys Res Space Phys 99(A3):3893–3914

Fuller-Rowell T, Millward G, Richmond A, Codrescu M (2002) Storm-time changes in the upper atmosphere at low latitudes. J Atmospheric Solar Terr phys 64(12–14):1383–1391

Gao Q, Liu L, Zhao B, Wan W, Zhang M, Ning B (2008) Statistical study of the storm effects in middle and low latitude ionosphere in the East-Asian sector (in Chinese). Chin J Geophys 51(3):435–443

Gonzalez W, Joselyn J-A, Kamide Y, Kroehl HW, Rostoker G, Tsurutani B, Vasyliunas V (1994) What is a geomagnetic storm? J Geophys Res Space Phys 99(A4):5771–5792

Gonzalez WD, Tsurutani BT, Clúa de Gonzalez AL (1999) Interplanetary origin of geomagnetic storms. Space Sci Rev 88(3):529–562

Gonzalez W, Guarnieri F, Yumoto K (2005). Global dayside ionospheric response to interplanetary electric fields: Plasma uplift and increases in total electron content. *Multiscale Coupling of Sun-Earth Processes*, pages 157–171

Grodji F, Doumbia V, Boka K, Amory-Mazaudier C, Cohen Y, Fleury R (2017) Estimating some parameters of the equatorial ionosphere electrodynamics from ionosonde data in West Africa. Adv Space Res 59(1):311–325

Habarulema JB, Katamzi ZT, McKinnell L-A (2013) Estimating the propagation characteristics of large-scale traveling ionospheric disturbances using ground-based and satellite data. J Geophys Res Space Phys 118(12):7768–7782

Habarulema JB, Yizengaw E, Katamzi-Joseph ZT, Moldwin MB, Buchert S (2018) Storm time global observations of large-scale TIDs from ground-based and in situ satellite measurements. J Geophys Res Space Phys 123(1):711–724

Hairston M, Coley W, Stoneback R (2016) Responses in the polar and equatorial ionosphere to the March 2015 St. Patrick Day storm. J Geophys Res Space Phys 121(11):11–213

Hajra R, Chakraborty S (2011) Equatorial ionospheric responses in relation to the occurrence of main phase of intense geomagnetic storms in the local dusk sector. J Atmospheric Solar Terr Phys 73(7–8):760–770

Heber B, Sanderson T, Zhang M (1999) Corotating interaction regions. Adv Space Res 23(3):567–579

Hobara Y, Lefeuvre F, Parrot M, Molchanov O (2005) Low-latitude ionospheric turbulence observed by Aureol-3 satellite. Ann Geophys 23(4):1259–1270

Horvath I, Lovell BC (2015) Positive and negative ionospheric storms occurring during the 15 May 2005 geomagnetic superstorm. J Geophys Res Space Phys 120(9):7822–7837

Hundhausen A (1999) Coronal Mass Ejections. Springer, Berlin

Ikubanni S, Adebiyi S, Adebesin B, Dopamu K, Joshua B, Bolaji O, Adekoya B (2018) Response of GPS-TEC in the African equatorial region to the two recent St. Patrick's day storms. Int J Civil Eng Technol 9(10):1773–1790

Iyemori T (1990) Storm-time magnetospheric currents inferred from mid-latitude geomagnetic field variations. J Geomagn Geoelectr 42:1249–1265

Iyemori T, Rao DRK (1996) Decay of the dst field of geomagnetic disturbance after substorm onset and its implication to storm-substorm relation. Ann Geophys 14:608–618

Kakad B, Nayak C, Bhattacharyya A (2012) Power spectral characteristics of ESF irregularities during magnetically quiet and disturbed days. J Atmospheric Solar Terr phys 81:41–49

Kashcheyev A, Migoya-Orué Y, Amory-Mazaudier C, Fleury R, Nava B, Alazo-Cuartas K, Radicella S (2018) Multivariable comprehensive analysis of two great geomagnetic storms of 2015. J Geophys Res Space Phys 123(6):5000–5018

Kelley M (1989) Ionospheric Radio. Peter Peregrinus Ltd., London

Kelley MC, Vlasov MN, Foster JC, Coster AJ (2004) A quantitative explanation for the phenomenon known as storm-enhanced density. Geophys Res Lett 31(19):1123

Kikuchi T, Hashimoto KK, Nozaki K (2008) Penetration of magnetospheric electric fields to the equator during a geomagnetic storm. J Geophys Res Space Phys 113(6):112

Kintner PM, Ledvina BM, De Paula E (2007) GPS Ionospheric Scintillations. Space Weather 5(9):1145

Kumar S, Veenadhari B, Chakrabarty D, Tulasi Ram S, Kikuchi T, Miyoshi Y (2020) Effects of IMF By on ring current asymmetry under southward IMF Bz conditions observed at ground magnetic stations: Case studies. J Geophys Res Space Phys 125(10):e2019JA027493

Lei J, Wang W, Burns AG, Solomon SC, Richmond AD, Wiltberger M, Goncharenko LP, Coster A, Reinisch BW (2008) Observations and simulations of the ionospheric and thermospheric response to the December 2006 geomagnetic storm: Initial phase. J Geophys Res Space Phys 113(1):112
Lin C, Richmond A, Heelis R, Bailey G, Lu G, Liu J-Y, Yeh H, Su S-Y (2005) Theoretical study of the low-and midlatitude ionospheric electron density enhancement during the October 2003 superstorm: Relative importance of the neutral wind and the electric field. J Geophys Res Space Phys 110(12):1123
Liu J, Zhao B, Liu L (2010) Time delay and duration of ionospheric total electron content responses to geomagnetic disturbances. Ann Geophys 28(3):795–805
Liu J, Liu L, Nakamura T, Zhao B, Ning B, Yoshikawa A (2014) A case study of ionospheric storm effects during long-lasting southward IMF Bz-driven geomagnetic storm. J Geophys Res Space Phys 119(9):7716–7731
Liu J, Wang W, Burns A, Yue X, Zhang S, Zhang Y, Huang C (2016) Profiles of ionospheric storm-enhanced density during the 17 March 2015 great storm. J Geophys Res Space Phys 121(1):727–744
Loewe C, Prölss G (1997) Classification and mean behavior of magnetic storms. J Geophys Res Space Phys 102(A7):14209–14213
Lühr H, Maus S, Rother M (2004) Noon-time equatorial electrojet: its spatial features as determined by the CHAMP satellite. J Geophys Res Space Phys 109(1):111
Luo W, Zhu Z, Xiong C, Chang S (2017) The response of equatorial ionization anomaly in 120°E to the geomagnetic storm of 18 August 2003 at different altitudes from multiple satellite observations. Space Weather 15(12):1588–1601
Manoj C, Maus S (2012) A real-time forecast service for the ionospheric equatorial zonal electric field. Space Weather 10(9):1–9
Manoj C, Maus S, Lühr H, Alken P (2008) Penetration characteristics of the interplanetary electric field to the daytime equatorial ionosphere. J Geophys Res Space Phys 113(12):1145
Matamba TM, Habarulema JB (2021) The ionospheric response to high-intensity long duration continuous AE activity (HILDCAA) event (13–15 April 2005) over mid-latitude African region. Adv Space Res 67(2):777–787
Matamba T, Habarulema J, McKinnel L-A (2015) Statistical analysis of the ionospheric response during geomagnetic storm conditions over South Africa using ionosonde and GPS data. Space Weather 13:536–547
McNamara LF (1991) Ionosphere Commun. Kriger Publishing Company, USA
Mendillo M (2006) Storms in the ionosphere: Patterns and processes for total electron content. Rev Geophys 44(4):1114
Mendillo M, Klobuchar JA, Hajeb-Hosseinieh H (1974) Ionospheric disturbances: Evidence for the contraction of the plasmasphere during severe geomagnetic storms. Planetary Space Sci 22(2):223–236
Molchanov OA (2004) On the origin of low-and middle-latitude ionospheric turbulence. Phys Chem Earth 29(4–9):559–567
Moldwin M (2008) Introduction Space Weather. Cambridge University Press, Cambridge
Nava B, Rodríguez-Zuluaga J, Alazo-Cuartas K, Kashcheyev A, Migoya-Orué Y, Radicella S, Amory-Mazaudier C, Fleury R (2016) Middle-and low-latitude ionosphere response to 2015 St. Patrick's Day geomagnetic storm. J Geophys Res Space Phys 121(4):3421–3438
Nayak C, Tsai L-C, Su S-Y, Galkin I, Caton R, Groves K (2017) Suppression of ionospheric scintillation during St. Patrick's Day geomagnetic super storm as observed over the anomaly crest region station Pingtung, Taiwan: A case study. Adv Space Res 60(2):396–405
Ngwira CM, McKinnell L-A, Cilliers PJ, Yizengaw E (2012) An investigation of ionospheric disturbances over South Africa during the magnetic storm on 15 May 2005. Adv Space Res 49(2):327–335
Nogueira P, Abdu M, Batista I, De Siqueira P (2011) Equatorial ionization anomaly and thermospheric meridional winds during two major storms over Brazilian low latitudes. J Atmospheric Solar Terr Phys 73(11–12):1535–1543
Omojola J, Adewumi T (2020) Effects of St Patrick's day intervals geomagnetic storms on the accuracy of GNSS positioning and total electron content over nigeria. J Earth Space Phys 45(4):181–188
Picanço G, Denardini C, Nogueira P, Barbosa-Neto P, Resende L, Chen S, Carmo C, Moro J, Romero-Hernandez E, Silva R (2021) Equatorial ionospheric response to storm-time electric fields during two intense geomagnetic storms over the Brazilian region using a Disturbance Ionosphere indeX. J Atmospheric Solar Terr Phys 223:105734
Prölss GW (1995) Ionospheric Reg storms. CRC Press, Boca Raton
Ren D, Lei J, Zhou S, Li W, Huang F, Luan X, Dang T, Liu Y (2020) High-speed solar wind imprints on the ionosphere during the recovery phase of the August 2018 geomagnetic storm. Space Weather 18(7):e2020SW002480
Rishbeth H (1963) Ionospheric storms and the morphology of magnetic disturbances. Planet Space Sci 11(1):31–43
Rishbeth H (1991) F-region storms and thermospheric dynamics. J Geomagn Geoelectr 43(Supplement1):513–524
Sahai Y, Becker-Guedes F, Fagundes P, De Jesus R, De Abreu A, Paxton L, Goncharenko LP, Brunini C, Gende M, Ferreira A et al (2009) Effects observed in the Latin American sector ionospheric F region during the intense geomagnetic disturbances in the early part of November 2004. J Geophys Res Space Phys. https://doi.org/10.1029/2008JA013053
Scherliess L, Fejer BG (1999) Radar and satellite global equatorial F region vertical drift model. J Geophys Res Space Phys 104(A4):6829–6842
Schunk R, Sojka JJ (1996) Ionosphere-thermosphere space weather issues. J Atmospheric Terr Phys 58(14):1527–1574
Seemala G, Valladares C (2011) Statistics of total electron content depletions observed over the South American continent for the year 2008. Radio Sci 46:1–14
Seemala G, Delay S.B (2010). GNSS TEC data processing. *2nd Workshop on Satellite Navigation Science and Technology for Africa, Trieste*, 6–24
Sekar R, Raghavarao R (1987) Role of vertical winds on the rayleigh-taylor mode instabilities of the night-time equatorial ionosphere. J Atmospheric Terr Phys 49(10):981–985
Shreedevi P, Choudhary R (2017) Impact of oscillating IMF Bz during 17 March 2013 Storm on the distribution of plasma over Indian low-latitude and mid-latitude ionospheric regions. J Geophys Res Space Phys 122(11):11–607
Simi K, Manju G, Haridas M, Nayar S, Pant TK, Alex S (2013) Ionospheric response to a geomagnetic storm during November 8–10, 2004. Earth Planets Space 65(4):343–350
Sugiura M (1963). Hourly values of equatorial Dst for the IGY. Technical report
Sugiura M, Kamei T (1991) Equatorial dst index 1957–1986. Int Assoc Geomagn Aeron Bull 40:1–246
Tesema F, Damtie B, Nigussie M (2015) The response of the ionosphere to intense geomagnetic storms in 2012 using GPS-TEC data from East Africa longitudinal sector. J Atmospheric Solar Terr Phys 135:143–151
Tsagouri I (2022) Space weather effects on the earth's upper atmosphere: short report on ionospheric storm effects at middle latitudes. Atmosphere 13(2):346
Tsurutani B, Mannucci A, Iijima B, Abdu MA, Sobral JHA, Gonzalez W, Guarnieri F, Tsuda T, Saito A, Yumoto K et al (2004) Global dayside ionospheric uplift and enhancement associated with interplanetary electric fields. J Geophys Res Space Phys 109(8):1112
Tulasi Ram S, Nilam B, Balan N, Zhang Q, Shiokawa K, Chakrabarty D, Xing Z, Venkatesh K, Veenadhari B, Yoshikawa A (2019) Three different episodes of prompt equatorial electric field perturbations under steady southward IMF Bz during St. Patrick's Day storm. J Geophys Res Space Phys 124(12):10428–10443
van der Meeren C, Oksavik K, Lorentzen D, Moen JI, Romano V (2014) GPS scintillation and irregularities at the front of an ionization tongue in the nightside polar ionosphere. J Geophy Res Space Phys 119(10):8624–8636
Vijaya Lekshmi D, Balan N, Tulasi Ram S, Liu J (2011) Statistics of geomagnetic storms and ionospheric storms at low and mid latitudes in two solar cycles. J Geophys Res Space Phys 116(11):111
Werner S, Bauske R, Prölss G (1999) On the origin of positive ionospheric storms. Adv Space Res 24(11):1485–1489
Yadav S, Sunda S, Sridharan R (2016) The impact of the 17 March 2015 St. Patrick's Day storm on the evolutionary pattern of equatorial ionization anomaly over the Indian longitudes using high-resolution spatiotemporal TEC maps: New insights. Space Weather 14(10):786–801

Yue X, Wang W, Lei J, Burns A, Zhang Y, Wan W, Liu L, Hu L, Zhao B, Schreiner WS (2016) Long-lasting negative ionospheric storm effects in low and middle latitudes during the recovery phase of the 17 March 2013 geomagnetic storm. J Geophys Res Space Phys 121(9):9234–9249
Zhang Y, Paxton L, Morrison D, Wolven B, Kil H, Meng C-I, Mende S, Immel T (2004) O/N2 changes during 1–4 October 2002 storms: IMAGE SI-13 and TIMED/GUVI observations. J Geophys Res Space Phys 109(10):1005
Zhao B, Wan W, Liu L (2005) Responses of equatorial anomaly to the October-November 2003 superstorms. Ann Geophys 23:693–706

Publisher's Note